Cloud based tool for analysis of chemical kinetic mechanisms

Nick J. Killingsworth*, Matthew J. McNenly, Russell A. Whitesides, Scott W. Wagnon

Lawrence Livermore National Laboratory, Livermore, CA 94550 USA

Abstract

The size and complexity of chemical kinetic models used to simulate combustion of hydrocarbon fuels continue to increase with our improved understanding of the underlying physical mechanisms, along with the improved ability to utilize such models as the result of increased computational power and efficiency. As mechanisms grow beyond thousands of species and tens of thousands of reactions, it becomes increasingly difficult to manually check for errors and physical inconsistencies. We present several automated methods to check for such issues in the specification of chemical reaction models. First, we demonstrate how discontinuities in thermodynamic data can cause simulation difficulties manifested as long wall-clock times and convergence failures. To correct this type of problem, we describe an automated method for refitting thermodynamic parameters. We also outline several methods to check the timescales of reaction rate coefficients to ensure physical consistency. All the methods are made available through a web-based tool (https://combustiontools.llnl.gov) intended to aid mechanism developers and users to improve the accuracy and performance of fuel models used by the combustion community.

Keywords:
Chemical Kinetics, Cloud Computing, Thermodynamics, Collision Theory

1. Introduction

There has been a marked increase in the use of more detailed physical models in reactive flow simulations, specifically more detailed combustion models and turbulence models [1, 2]. These additions are made possible due to widespread access to high performance computing resources and improved algorithms [3]. Detailed reaction mechanisms for the oxidation of large hydrocarbon fuels yield more accurate predictions of ignition and emissions phenomena [4]. While the most detailed reaction models now exceed thousands of species and tens of thousands of reactions [5, 6], even those with a few hundred species can have over ten thousand individual model parameters in the thermodynamic and reaction rate coefficient definitions. As such, it is nearly impossible to manually inspect the model specifications for typos or systematic errors. The consequences of reaction model errors have been highlighted in a recent paper [7], in which the authors surveyed twenty mechanisms in five consecutive issues of Combustion and Flame and found that 75% of the mechanisms contained reaction coefficients in excess of binary collision limits. The authors included a recommendation that all mechanisms should be checked for such violations and a corresponding report should be included with submissions for publication. The method outlined in [7] has been implemented by Yalamanchi et al. [8] in a web-based tool to check bimolecular reaction rate coefficients. Yalamanchi et al. [8] also present a procedure to use computational singular perturbation to identify ultrafast time scales in chemical mechanisms. In another recent publication [9], an automated tool was used to compare reaction rate coefficients and thermochemistry for butanol across 74 published chemical mechanisms, and significant differences were found. The same study also showed how reaction rate coefficients can mutate as they are tuned for specific targets.

This paper outlines a set of tools developed to address errors and numerical challenges in chemical mechanisms that have been identified by other authors. Additionally, this work addresses some issues that have not been reported before, but that have been identified as common problems in published models. All the tools have been incorporated into a web application (`https://combustiontools.llnl.gov`) to aid the community in identifying errors in their chemical mechanisms and the associated thermodynamic files. Cloud computing is a promising technology to help researchers share the tools they have developed to improve the quality of chemical mechanisms and aid in collaboration [10, 11]. Cloud computing has several benefits: it allows utilization of a consistent database maintained by a single administrator, new users can quickly start using tools and submitting data without having to install software, and a single developer can push updates that add features and improve performance for all users.

There are two general types of problems that our tools address, issues in the specification of thermodynamic properties, and issues in the specification of reactions and rate coefficients. Thermodynamic property data are required for evaluating chemical system state and equilibrium reverse reaction rate coefficients [12]. We discuss common problems with thermodynamic

*Corresponding author:
Email address: `killingsworth2@llnl.gov` (Nick J. Killingsworth)

property specification and our automated solutions in Section 2. In Section 3 we discuss issues that arise in the specification of chemical reactions and reaction rate coefficients and our tools to help identify and correct such problems.

2. Thermochemistry Error Identification and Correction

The calculation of thermodynamic properties is a key component in simulating chemical systems and determining how accurately a model describes the real system [6, 12, 13]. Thermodynamic properties are used to determine the state of the system and in the calculation of certain reverse reaction rate coefficients from equilibrium. They can also impact the numerical methods used in simulations, where functional issues such as discontinuities in the temperature dependence can impact the CPU/wall-time it takes to reach a solution. In zero-dimensional reactor simulations, the time integration method may reduce the time-step by several orders of magnitude in an attempt to resolve the discontinuity, leading to an unnecessary increase in the computational cost. In some cases, the time step reduction results in convergence errors leading to solution failure or erroneous results. The effect of thermochemical discontinuities on the ODE time step during simulations of a constant volume homogeneous zero-dimension ignition delay calculation using the Zero-RK solver [3] are shown in Fig. 1. Here stoichiometric auto-ignition of a toluene reference fuel (TRF) is simulated with initial temperature and pressure of 800 K and 25 bar, respectively. Fuel composition was set as 38.7 volume % isooctane, 20.1 volume % n-heptane, and 41.3 volume % toluene to match a RON of 91.5 and sensitivity of 7.5 based on [14], and a 137 species reaction model [15] was used. As the temperature approaches a discontinuity in the thermodynamic functions at 1000 K the solver drastically reduces the time step from around $10^{-6} s$ to $10^{-11} s$. Also shown is a simulation run with the discontinuities removed (labeled Refit) where no time step reduction is necessary. The refit thermodynamic data leads to a 10% reduction in simulation wall-clock time with less than 0.053% change in the computed ignition delay. The impact of a given discontinuity in the thermodynamic functions and resultant improvement on simulation wall-clock time will depend on the size of the discontinuity, the specific species, and the chemistry solver used. The approach used to remove the discontinuous thermodynamic properties is described in the following subsection. Boettcher *et al.* [16] and Cuoci *et al.* [17] outline two slightly different methods of automatically correcting thermodynamic functions.

2.1. Thermodynamic Properties

Combustion models often calculate thermodynamic properties based on empirical polynomial equations pioneered by researchers at NASA [18]. Use of these equations assumes the species are always in thermodynamic equilibrium and therefore only a function of temperature. To improve the empirical fit, two temperature ranges defined by three temperatures (T_{low} to T_{mid} and T_{mid} to T_{high}) are used. Typical values for T_{low}, T_{mid}, and T_{high} are 300, 1000, and 5000 K, respectively. For each

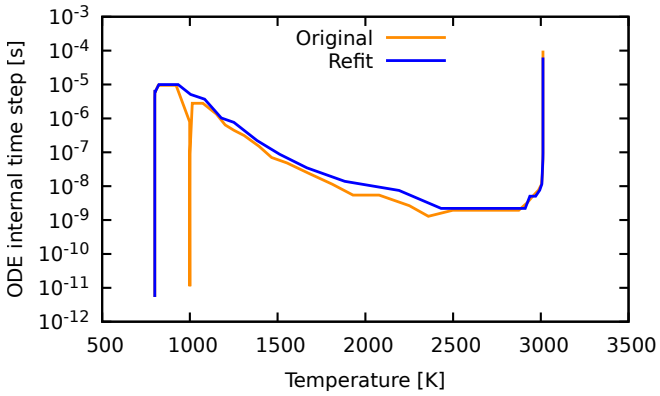

Figure 1: The effect of discontinuous thermodynamic properties on the simulation of a constant volume, zero-dimension reactor. Discontinuities cause the solver to reduce the time step, removing the discontinuities results in a 10% faster simulation time.

species and each temperature range, seven polynomial coefficients are specified, which are generally found by fitting the model to measured data or theoretical results [19]. Heat capacity at constant pressure C_p°, enthalpy H°, and entropy S° are modeled as functions of temperature T in Kelvin using the polynomial coefficients a_n. Here $a_1, \ldots, a_5$ capture the temperature dependence, a_6 relates to the enthalpy of formation at standard conditions, and a_7 relates to the entropy of formation at standard conditions.

$$\frac{C_p^\circ}{R} = a_1 + a_2 T + a_3 T^2 + a_4 T^3 + a_5 T^4, \tag{1}$$

$$\frac{H^\circ}{RT} = a_1 + \frac{a_2}{2} T + \frac{a_3}{3} T^2 + \frac{a_4}{4} T^3 + \frac{a_5}{5} T^4 + \frac{a_6}{T}, \tag{2}$$

$$\frac{S^\circ}{R} = a_1 \ln(T) + a_2 T + \frac{a_3}{2} T^2 + \frac{a_4}{3} T^3 + \frac{a_5}{4} T^4 + a_7, \tag{3}$$

where R is the universal gas constant. Other thermodynamic properties needed in combustion simulations can be derived from these quantities [20].

Without particular attention, it is easy to define the polynomial coefficients such that the values of Eqs. (1-3) at $T = T_{mid}$ for the two temperature ranges will not be equal, resulting in a discontinuity. From the TRF mechanism of Andrae *et al.* [15], the specific heat of 1,3-pentadiene, $CH_2CHCHCHCH_3$ exhibits this type, as shown in Fig. 2. Such discontinuities are commonplace in published models. A review of the thermodynamic files for 14 of the mechanisms surveyed by Chen et al. [7] were analyzed and 13 exhibited discontinuities at $T = T_{mid}$ of at least one thermodynamic property C_p/R, H/RT, or S/R of greater than 0.1 in non-dimensional units for at least one species and often for between tens and hundreds of species, a value of 0.1 is typically large enough to impact the solver.

2.2. Correcting Thermodynamic Discontinuities

The following algorithm is proposed to ensure thermodynamic properties and their first derivatives with respect to tem-

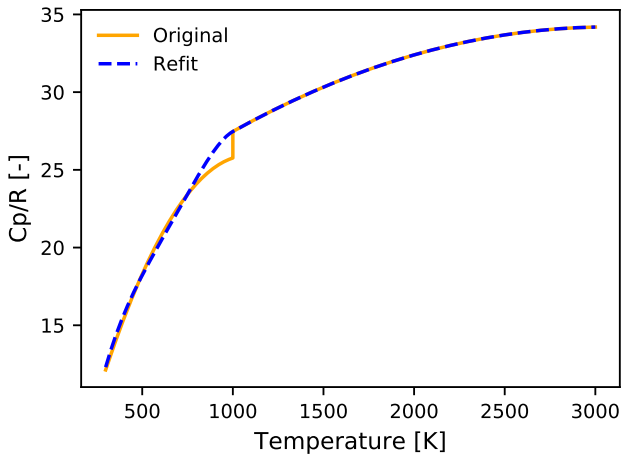

Figure 2: The non-dimensional heat capacity for 1,3-pentadiene, the largest discontinuity found in the 137 species TRF surrogate mechanism [15].

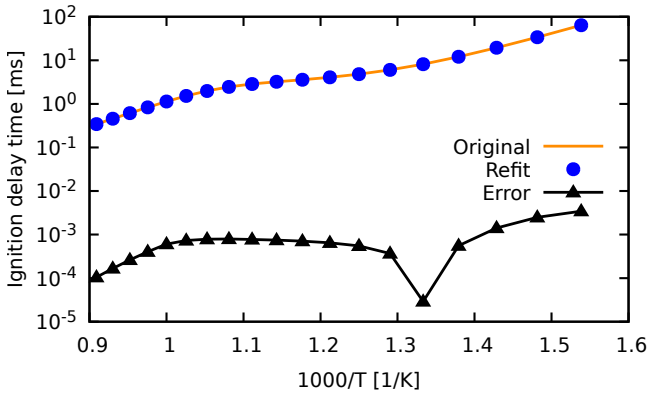

Figure 3: Comparison of ignition delay time as a function of temperature for original TRF surrogate and the updated mechanism with refit, continuous thermochemistry data, as well as the absolute error in computed ignition delay between the two.

perature are continuous; specifically, they are C_0 and C_1 continuous, at $T = T_{mid}$. First, new lower branch coefficients $a_1 - a_5$ are found using a least squares regression to minimize the error between the heat capacity with the original coefficients and with the new coefficients with the following constraints,

1. Heat capacity at T=298.15 K matches that found with the original lower branch coefficients.
2. Heat capacity at $T = T_{mid}$ matches that found with the original higher branch coefficients.
3. The derivative of the heat capacity at $T = T_{mid}$ matches that found using the original higher branch coefficients.

Next a_6 for the lower branch is chosen such that the enthalpy at T=298.15 K matches that found using the original lower branch coefficients. The high temperature branch value for a_6 is then adjusted so that the enthalpy for both branches matches at $T = T_{mid}$. The same procedure is then carried out for the entropy parameter a_7. The value for the lower temperature branch is chosen such that the entropy at T=298.15 K matches that found using the original lower branch coefficients, and the higher branch value for a_7 is set such that the entropy for both branches matches at $T = T_{mid}$.

Constant volume, adiabatic ignition delay times were simulated for a TRF mixture using the Andrae *et al.* mechanism [15] before and after refitting of the thermochemistry parameters by the above algorithm. The resulting data are plotted versus initial temperature in Fig. 3 for the original and refit thermochemistry. The absolute error induced by the refitting is also plotted in Fig. 3, showing that for these simulations the change in ignition delay time as a result of this process is less than 0.1% across the sweep. Note that while we highlighted a particularly noticeable discontinuity for a single species in this mechanism, any function evaluation that results in a discontinuity in the time derivative greater than the numerical integrator tolerances will most likely increase the overall simulation cost.

The impact of thermodynamic discontinuities can grow substantially for reacting flow simulations (e.g. computational fluid dynamics with operator splitting), every time the thermodynamic state in a fluid dynamic cell *or* reacting zone crosses a discontinuity (at $T = T_{mid}$ for some species) the solver time step can drop from 10^{-7} s to 10^{-13} s or smaller. The time penalty can be even worse for simulations with reacting cells or zones that are fully coupled by the species transport equations or even through the equation of state. When coupled zones evolve along different temperature histories, it increases the likelihood of multiple discontinuity traversals occurring at different times, each requiring separate reductions in the time-step. This behavior is investigated with a slider-crank multi-zone model with the zones fully-coupled through a common cylinder pressure [21]. The 1,400-species gasoline surrogate mechanism from [22] is used with a charge equivalence ratio of 0.2, and compression ratio of 17.5. Simulations are run to quantify the impact of the original and refit thermochemistry as a function the number of reacting zones representing the trapped charge in the cylinder. Figure 4 shows the temperature as a function of crank angle for each of the zones in a four-zone simulation. Note that each zone passes through discontinuities at 1000 K at different times. The wall clock time for these simulations is given in Fig. 5, which shows that the simulations using the refit thermochemistry have a reduction in computation cost of up to four times for the largest number of zones tested.

2.3. *Thermodynamics of Isomers*

Experimental thermochemical data exists for many stable species and has been compiled in databases such as [23]; however, data for species with shorter lifetimes such as radicals are difficult to obtain experimentally. For these species, we more often rely on ab initio calculations [24, 25, 26] or estimates such as group additivity with hydrogen bond increments. Here, we show that plotting thermodynamic data for isomers together can be an efficient way to visualize data for many species, and can be an effective way to discover errors by looking for outliers. The tendency for isomers to have similar thermodynamic behavior to each other can be understood by considering the group additivity concept [27, 28]. In this method, thermody-

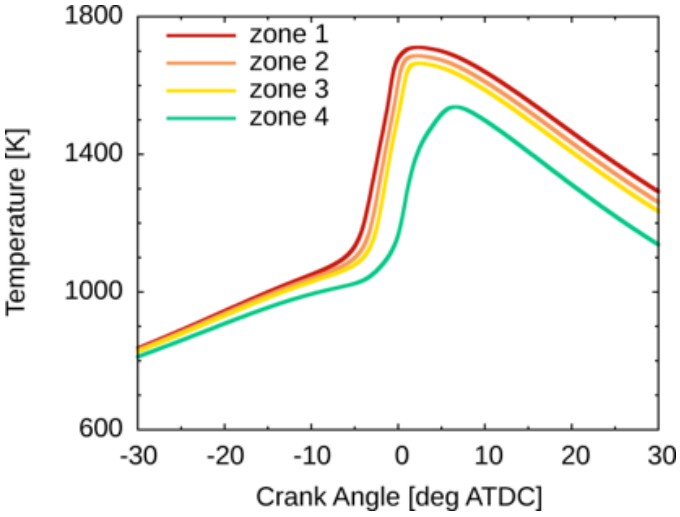

Figure 4: Temperature traces for four zone slider crank simulation, illustrating that the zones traverse discontinuities at different times, each leading to an increased computational cost for the simulation.

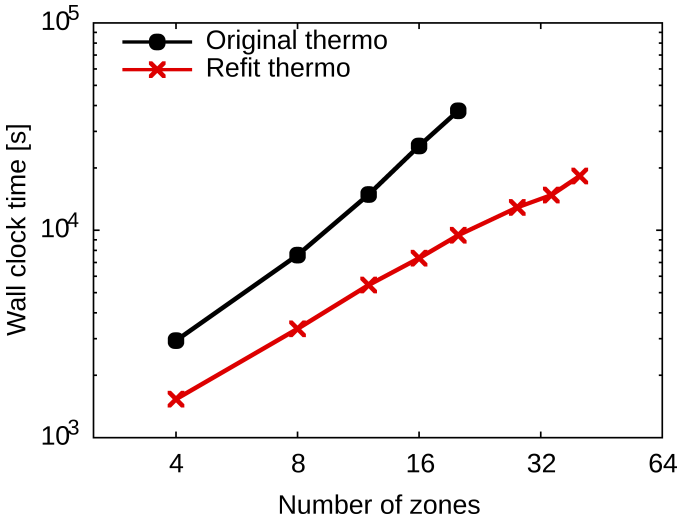

Figure 5: Comparison of the user wait-time (or wall-clock time) for the multizone simulations using the original discontinuous (circles) and the refit thermodynamics (exes).

namic behavior is approximated by assuming that to zeroth order thermodynamic properties are based on the atoms that make up the molecule, to first order by the bond properties, and to second order on group properties. Isomers all contain the same atoms so to zeroth order are equivalent. There will be some discrepancies for the first and second order assumptions, but many primary bonds are the same, as well as, groups. Based on these assumptions we can expect isomers to generally have similar thermodynamic behavior. Thus, if we see significant deviations in thermodynamic properties between isomers it is worth confirming that the parameters have been specified correctly.

To illustrate this method, we use thermodynamic data for selected isomers of C_8H_{17} (iso-octane with a hydrogen atom removed) from [24] in which *ab initio* computational methods were used to estimate the radicals' heat capacity at constant pressure and entropy as a function of temperature. The plots in Fig. 6 show that the thermodynamic values are close for each of the isomers.

Similarly, Fig. 7 shows a plot of heat capacity at constant pressure for isomers of C_6H_{12} from [23]. This plot shows that even isomers with very different structures can have similar thermodynamic behavior.

The thermodynamic diagnostic on the Combustion Tools website (https://combustiontools.llnl.gov/) automatically plots the heat capacity, enthalpy, and entropy as a function of temperature for all isomers in the thermodynamic files with each other so that the user can easily compare their behavior and determine if there are any outliers. To test this functionality, we used the Combustion Tools website to plot the isomers for the thermodynamic data for a large methyl decanoate mechanism [29] with 2878 species, this resulted in 201 sets of plots. Scanning through the plots an isomer of $C_8H_{16}O$ stood out as having different behavior at higher temperatures than its isomers, see Fig. 8. We recomputed the thermodynamic parameters for this species using group additivity and the revised thermodynamic parameters match the other isomers well. This example shows

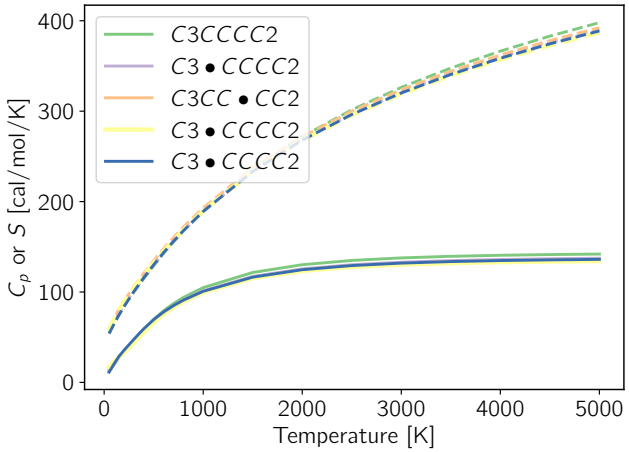

Figure 6: Heat capacity at constant pressure (solid) and entropy (dashed) as a function of temperature for C_8H_{17} isomers calculated using *ab initio* computational methods [24].

how the tool can be used to quickly scan large mechanisms for bad thermodynamic parameters.

3. Chemical Mechanism Checks

Over the course of testing and using various combustion chemistry mechanisms we have identified a number of common issues and have devised checks to flag and sometimes fix such problems. The first set of analyses described in the next section outlines several basic checks that are used to identify species that may cause numerical issues or are erroneously specified in the reaction network. The latter section focuses on analyzing reaction rate coefficients and identifying if they are unphysical.

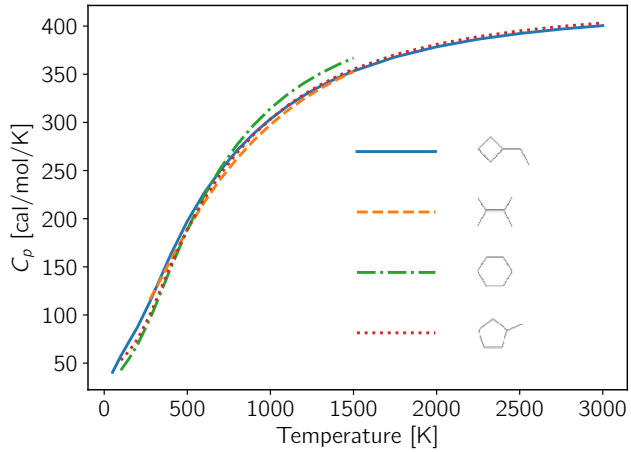

Figure 7: Heat capacity at constant pressure for isomers of C_6H_{12} from [23].

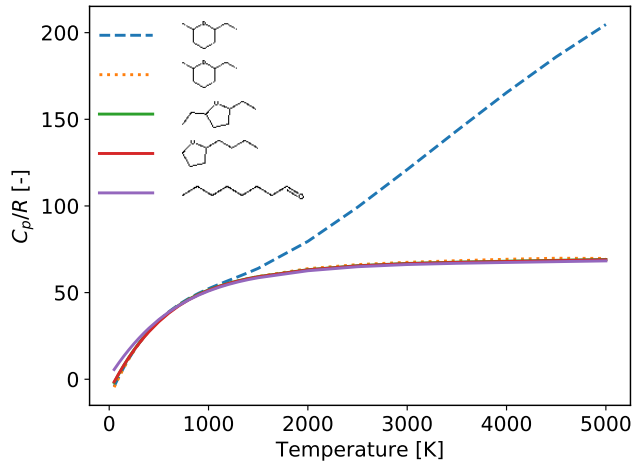

Figure 8: Heat capacity at constant pressure for isomers of $C_8H_{16}O$ from [29]. The thermodynamic parameters for the outlier isomer (blue dashed line) were recomputed and the refit (orange dotted line) results in behavior similar to the other isomers.

3.1. Basic Mechanism Checks

Basic checks are conducted on the species in the mechanism file to determine how many and what types of reactions in which each species participates. A basic network analysis is conducted to see if there are species that are not included in any reactions or participate in ways that are unphysical. The number of reactants and products for each reaction are tabulated, this information can be useful to determine if there are forward or reverse reactions that involve more than three reactants, which are unlikely to collide in reality. Additionally, species that fall under any of the following categories are flagged and tabulated,

1. *Adduct-Only Species* is a species that is the only reactant in all reaction steps in which it is involved. More broadly, an adduct species is a single new species resulting from the direct combination of two separate initial species. However, species flagged under this category only participate in unimolecular reaction steps and do not participate in bimolecular reaction steps. Such species are more likely to exist for nonphysical short or long time scales.
2. *Lone Reaction Species* is a species that only appears in a single reversible reaction step.
3. *Source Species* is a species that only appears as a reactant in irreversible reaction steps. Such a species may be defined in the initial composition but will only decrease in quantity as there is no path for production.
4. *Sink Species* is defined as a species that only appears as a product in irreversible reaction steps. It will only increase in quantity.

3.2. Reaction Rate Coefficient Analysis

Chemical kinetics of combustion systems are governed by a wide range of time scales. For complex hydrocarbon fuels at typical flame conditions, unimolecular dissociation reactions can have characteristic frequencies around $10^{14}s^{-1}$, while the global heat release controlling reactions are typically much slower ($10^6 s^{-1}$). The disparity in time scales, quantified by the ratio of the fastest to slowest time scales, is a measure of the stiffness of the system and relates to how difficult the system is to integrate. Thus, identifying and correcting faster-than-physical rates can reduce the computational cost. Procedures for identifying the system's characteristic time scales are explained in this section. We first examine unimolecular reaction rate coefficients, then compare binary reaction rate coefficients to those calculated using collision theory. Finally, we use the system Jacobian calculated by the implicit numerical integrator to gain information about the chemical system's time scales, which covers higher order reactions not included in the analysis of unimolecular and bimolecular reactions.

3.2.1. Unimolecular Reaction Rate Coefficients

A unimolecular reaction is a reaction in which a single reactant undergoes a chemical change resulting in one or more products. For the purpose of checking unimolecular reaction rate coefficients an algorithm is implemented to check those reactions that depend solely on temperature and excludes reactions that explicitly involve another particle or are pressure dependent. The rate coefficients are computed across a range of user-specified temperatures spanning the combustion regime of interest (default range is 300 K to 3000 K). The computed rate coefficients are sorted from the fastest to slowest and those above a user-specified threshold are reported allowing further investigation. The default rate coefficient threshold value is calculated based on conventional transition state theory. The general conventional transition state theory equation to evaluate rate coefficients is [30],

$$k^{\ddagger}(T) = \gamma(T)\frac{k_B T}{h}\left(\frac{RT}{p^{\circ}}\right)^{m-1} exp\left(\frac{\Delta S^{\ddagger,\circ}}{R}\right) exp\left(\frac{-\Delta H^{\ddagger,\circ}}{RT}\right), \quad (4)$$

where, $\gamma(T)$ is the transmission coefficient, k_B is the Boltzman constant with units [J/K], h is Plank's constant with units [Js],

p° is standard pressure, typically 101,325 Pa, m is the molecularity *i.e., unimolecular = 1, bimolecular = 2*, $\Delta S\ddagger$ is the change in entropy, $S\ddagger - S_{reactants}$ in [J/mol K], and $\Delta H\ddagger$ is the change in enthalpy, $H\ddagger - H_{reactants}$ in [J/mol]. For the unimolecular rate coefficient, we can take a molecularity of one. Assuming a transmission coefficient of unity and that the changes in entropy and enthalpy are zero (i.e. the transition state is indistinguishable from the reactant) we arrive at a conservative threshold for the rate coefficient,

$$k^{\ddagger}(T) = \frac{k_B T}{h}, \tag{5}$$

which varies linearly from $6\text{x}10^{12} s^{-1}$ at 300 K to $6\text{x}10^{13} s^{-1}$ at 3000 K.

3.2.2. Binary Collision Rate Comparison

Bimolecular reactions involve two particles (molecules, radicals, ions) that come into contact and both undergo a chemical change [6]. For these reactions to occur, the molecules must first collide. Thus, the collision rate between two species is expected be greater than the rate at which those two molecules are consumed in a reaction. Comparing calculated bimolecular reaction rate coefficients to estimated collision rate coefficients for pairs of species helps indicate reactions with unphysically large rate coefficients. Chen *et al.* [7] performed a similar check by computing the maximum ratios of rate coefficients with respect to the collision limit for a number of temperatures. In that work, they used kinetic theory along with molecular specific properties from transport databases provided with mechanisms to estimate the bimolecular collision rates. When transport databases were not provided with the mechanisms they used a constant collision rate coefficient of $2.9 \times 10^{15} \frac{cm^3}{mol\, s}$ which corresponds to the collision rate coefficient for H and n-dodecane at 2500 K. In this work we also use kinetic theory to estimate the bimolecular collision rate coefficient for each combination but utilize methods of determining the molecular specific properties that do not require the user to supply a transport database as outlined in the following section. The binary collision rate is only used as an approximate upper limit on the rate coefficients. The difference between user supplied or estimated transport properties is not expected to be significant in flagging reaction rate constants for further inspection. The use of user specified transport properties may be added in the future.

The binary collision rate depends on the number of molecules, their speed, and size. If the molecules interact with each other like billiard balls, or hard spheres, it is straightforward to compute the binary collision rate from kinetic theory. Specifically, the collision rate $Z_{AB} = z_{AB} n_A n_B$ between molecules A and B is proportional to the number of A and B molecules per unit volume, n_A and n_B respectively. The binary collision rate coefficient z_{AB} is calculated from [31] as

$$z_{AB} = \frac{d_{AB}^2}{\kappa_{AB}} \left(\frac{8\pi k_B T}{M_{AB}^*} \right)^{\frac{1}{2}}, \tag{6}$$

where k_B is the Boltzmann constant and T is the temperature. M_{AB}^* is the reduced mass of the colliding molecules and is defined as,

$$M_{AB}^* = \frac{M_A M_B}{M_A + M_B}, \tag{7}$$

where M_n is the molecular weight of species n. κ_{AB} is a symmetry factor that is 1 when $A \neq B$ and 2 when $A = B$. d_{AB} is the average hard sphere diameter of the two molecules A and B. Real molecules do not, however, interact as hard spheres. The effective size, or collision cross-section, varies depending on the quantity being transported by the molecules (*i.e.*, mass, momentum, or energy). Further, the cross-section typically changes with the relative speed of the colliding molecules, which increases, in an average sense, with the equilibrium temperature of the fluid. Following the variable hard sphere approximation of [32], the collision cross-section variation is proportional to $T^{1/2-\omega}$, where *omega* is the power-law temperature exponent of the viscosity for the gas mixture. For most gases $1/2 < \omega < 1$ meaning that the largest factor by which the cross-section could change from 300 K to 3000 K is only three if $\omega = 1$. Since the collision rate coefficient only needs to be approximate for error detection, the temperature dependence of the cross-section is ignored, and the hard sphere binary collision rate coefficient given in (6) is used with the following ansatz. The hard sphere diameter of each molecule is computed at a reference temperature of $T_{ref} = 1000$ K from [32],

$$d_n = \left(\frac{5}{16 \mu_{ref}} \left(\frac{M_n k_B T_{ref}}{\pi N_A} \right)^{\frac{1}{2}} \right)^{\frac{1}{2}}, \tag{8}$$

where μ_{ref} is the reference dynamic viscosity in [Pa s] at the reference temperature, and N_A is Avogadro's number. μ_{ref} is estimated for each species based on the first order approximation from Chapman-Enskog theory [33] assuming a Lennard-Jones (LJ) 12-6 potential between molecules,

$$\mu_{ref} = \frac{5}{16} \frac{(\pi M_n k_B T)^{\frac{1}{2}}}{\pi \sigma^2 \Omega^{(2,2)}}, \tag{9}$$

Here σ is the finite, zero potential distance between the molecules, ϵ is the potential well depth between the molecules, and $\Omega^{(2,2)}$ is the dimensionless collision integral for viscosity evaluated at T_{ref}/ϵ The collision integral $\Omega^{(2,2)}$ is found by interpolating the theoretical results from [34] in Table E.2 of [33]. While Eq. 9 was derived for monatomic gases it has been found to work well for polyatomic gases [33].

Combining equations (6 - 9), the binary collision rate coefficient estimate becomes

$$z_{AB} = \frac{\sigma_{AB}}{\kappa_{AB}} \left(\frac{8\pi k_B T}{M_{AB}^*} \right)^{\frac{1}{2}} \Omega^{(2,2)} \left(\frac{T_{ref}}{\epsilon_{AB}} \right). \tag{10}$$

The resulting equation is almost the same as equation (1) in Chen *et al.* [7] except that the nondimensional collision integral $\Omega^{(1,1)}$ for mass transport is used there instead of $\Omega^{(2,2)}$, which is related to momentum transport. The other key difference is that the temperature dependence of the collision integral term

is replaced by a single evaluation at T_{ref} in this study. The motivation of using a single collision integral temperature, and assuming an effective hard sphere collision cross-section at T_{ref}, is to simplify the temperature dependence in (10). This allows for the rapid evaluation of the binary collision rate coefficient, which can be used as a real-time limiter during the integration of complex chemistry systems. To complete the collision rate coefficient estimate, the Lennard-Jones parameters are needed for each species. They are obtained using an internal database for common small species (*e.g.*, H_2, N_2, O_2, and H_2O) based on published data [35], and a simple molecular weight correlation proposed by Wang and Frenklach [36]. The website reports the following calculated values for each species in the mechanism file: LJ parameters σ and ϵ, viscosity at T_{ref}, μ_{ref} and the estimated hard sphere diameter. A comparison is made by taking the ratio of the reaction rate coefficient (converted from units of $[\frac{m^3}{kmol\,s}]$ to $[\frac{m^3}{particles\,s}]$) to the estimated collision rate coefficient. A report is then generated of estimated collisional rate coefficient for each reaction over the specified temperature range. A default pressure of 6 MPa is used to calculate the reaction rate coefficients, which only impacts pressure-dependent rate coefficient expressions. The binary collision rate coefficients for all the binary reactions are sorted from highest to lowest and listed for all the temperatures tested. Given the approximate nature of the collision rate coefficient determination, those ratios greater than one should be viewed as suspect, and the reaction rate coefficients should be investigated.

3.2.3. Jacobian Based Analysis

The previous two sections present methods to check the reaction rate coefficients of unimolecular and bimolecular reactions, covering the majority of reactions in typical combustion mechanisms. However, mechanisms also generally contain higher order and pressure dependent reactions that are not covered by those methods. In this section, we make use of timescale information taken from the Jacobian of the governing differential equations describing the evolution of the thermodynamic state and composition of a simple, homogenous reactor. Not only do very fast Jacobian timescales indicate nonphysical reactions, they also provide insight into potential challenges faced by the numerical integrator that can unnecessarily increase the computational cost of simulating the combustion system.

The Jacobian is used during implicit integration of the governing differential equations and contains the gradients of the system's time derivatives in thermodynamic and composition space. It contains local information about the system's time scales at any moment in time. As the Jacobian is calculated during integration of a chemical system, the associated time scale information is available at no extra computational cost. To take advantage, we monitor the terms that contribute to each element of the Jacobian matrix during a constant volume homogenous 0-D reactor model like those described in Section 2 and described in more detail in [3, 22]. The homogenous 0-D reactor is commonly used to model ignition behavior and is a prevalent sub-model in multi-dimensional combustion simulations [37, 38, 3]. In the adiabatic homogenous 0-D reactor model, the chemical mechanism defines the differential equations governing the rate of change of species concentrations, and the system's state is fully specified by two thermodynamic properties and the species concentrations. In this work, we use temperature T, relative volume v, and species mass fractions y_i for $1 \leq i \leq N_s$, where N_s is the number of species, and relative volume is held constant. Thus, the ordinary differential equations describing the change in species mass fractions and temperature with time (see [39]) are,

$$\frac{dy_i}{dt} = vM_i\dot{\omega}_i, \text{ and} \tag{11}$$

$$\frac{dT}{dt} = -\frac{1}{\bar{c}_v}\sum_{i=1}^{N_s} u_i\frac{dy_i}{dt}, \tag{12}$$

where M_i is the molecular mass of species i, and $\dot{\omega}_i$ is the net molar production rate of species i. In Eq. (12), $\bar{c}_v$ is the mixture-averaged, constant volume specific heat per unit mass and u_i is the specific energy of species i per unit mass. The mixture is assumed to be an ideal gas with the temperature dependence of $c_{v,i}$ accounted for using Eq. (1) and the relationship $c_v = c_p - R$. The energy, u_i, is calculated by integrating the polynomial fit for $c_{v,i}$ with the appropriate offset for heat of formation.

The net molar production rate $\dot{\omega}_i$ is computed as

$$\dot{\omega}_i = \sum_{j=1}^{N_r}\left(\nu''_{i,j} - \nu'_{i,j}\right)\psi_j, \tag{13}$$

where N_r is the number of uni-directional reaction steps, ψ_j are the reaction rates of progress, and $\nu''_{i,j}$ and $\nu'_{i,j}$, are the product and reactant stoichiometric coefficients for reaction step j, respectively. The reaction rate ψ_j of a uni-directional reaction step is defined in terms of the species molar concentration as,

$$\psi_j = k_j\prod_{i=1}^{N_s} C_i^{\nu'_{i,j}}, \tag{14}$$

where the molar concentration of species i is $C_i = y_i/vM_i$ and the rate coefficient k_j in Eq. (14) can be a function of temperature, pressure and individual species concentrations in the case of enhanced third-body reactions. However, most reactions found in detailed fuel mechanisms use a rate coefficient with a modified Arrhenius form that is only dependent on temperature. The reaction order of each reaction step j is the sum of the exponents $\nu'_{i,j}$ in Eq. (14) and is not necessarily equal to the molecularity of the reaction as lumping of elementary reactions can cause a difference between the two.

Having laid out the definition of the homogenous 0-D reactor model, we return to how we use the system's Jacobian to analyze reaction rates during integration. The Jacobian matrix, J, for a general N-dimensional ODE system, $dx_i/dt = f_i(x_1, \ldots, x_N, t)$ for $1 \leq i \leq N$, is defined as $J_{ij} = \partial f_i/\partial x_j$. Thus, the Jacobian matrix for the homogenous 0-D reactor sys-

tem Eqs. (11-12) ordered $(y_1, \ldots, y_N, T)$ is,

$$J_{ij} = \begin{cases} \frac{M_i}{M_j}\frac{\partial \dot{\omega}_i}{\partial C_j} & \text{for } 1 \le i, j \le N_s \\ \frac{1}{\nu M_j}\frac{\partial f_T}{\partial C_j} & \text{for } i = N_s + 1,\ 1 \le j \le N_s \\ \nu M_i \frac{\partial \dot{\omega}_i}{\partial T} & \text{for } 1 \le i \le N_s,\ j = N_s + 1 \\ \frac{\partial f_T}{\partial T} & \text{for } i = j = N_s + 1 \end{cases} \tag{15}$$

where the function f_T is the temperature time derivative defined in Eq. (12).

The chemical system's time scales at each time step during integration are defined by the Jacobian's eigenvalues. However, it is computational expensive to compute the eigenvalues every time step, so we make use of the Gerschgorin circle theorem to obtain estimates of the eigenvalues and therefore of the system time scales. The Gerschgorin circle theorem states that every eigenvalue of an *mxm* matrix A lies within a circular disc in the complex plane, where each disc is centered about one of the diagonal entries a_{ii} of the matrix A and the radius of each disc is equal to the sum of the absolute value of the elements of the corresponding row excluding the diagonal element $R_i = \Sigma_{j \neq i}|a_{ij}|$ [40]. A large diagonal term a_{ii} indicates that the center of one of the Gerschgorin discs has a large value and the matrix may have a large eigenvalue. Similarly, a large off-diagonal term (a_{ij} where $j \neq i$) indicates the radius of a Gerschgorin disc is large and the corresponding eigenvalue may be large. This can be used to identify reactions involved in fast eigenmodes of the chemical system by examining all terms that make up the Jacobian's elements and flagging any large values. These large individual terms indicate a reaction may be producing a large eigenvalue and therefore a fast mode of the system. It is important to stress that this analysis of each term in each element of the Jacobian can produce false positives in the case where two large reaction terms cancel each other. Consequently, this method does not prove that there is an unphysically fast eigenmode, but indicates that there may be one and, in our experience, it has been helpful for identifying if a bad reaction is responsible for it.

To see how the elements of the Jacobian contain information about the time scales of the system we can look at the first term in Eq. (15), $\frac{M_i}{M_j}\frac{\partial \dot{\omega}_i}{\partial C_j}$. The net molar production rate $\dot{\omega}$ has units $\frac{kmol}{m^3 s}$ and the species concentration C has units $\frac{kmol}{m^3}$, thus the units of $\frac{M_i}{M_j}\frac{\partial \dot{\omega}_i}{\partial C_j}$ are 1/s. The units of temperature similarly cancel to yield the term J_{ij} when $i = j = N_s + 1$. To eliminate the concentration and temperature units in the remaining terms, a reference temperature of 1000 K and a reference concentration equal to p_0/RT_0 are used to normalize the values. Here p_0 and T_0 are the user-specified initial temperature and pressure of the homogenous reactor. This step ensures that all terms in the Jacobian have the same units and approximate scale. If instead the local state is used rather than constant values for temperature and concentration there will be added variation to these terms making comparison from a given time to another more difficult.

To explore the type of information this analysis yields, we examine a detailed mechanism for n-heptane with 654 species and 2,827 reactions [41] during an ignition calculation of a stoichiometric mixture initiated at a temperature of 800 K and pressure of 20 bar. A plot of the temperature and pressure history are shown in Fig.9 (a). We use the peaks in the derivative of the temperature with respect to time to determine the timing of low- and high-temperature ignition as 0.686 ms and 1.143 ms, respectively. Plots in Figs.9 (b)-(d) show the distribution of Jacobian summands at the time of low temperature ignition, hot ignition, and after hot ignition as indicated in Fig.9 (a). Each bar represents the total sum of terms per decade of the magnitude of the Jacobian's elements in Eq. (15), categorized by reaction type, as well as, the temperature derivative terms.

We check the mechanism's time scales by comparing the magnitude s^{-1} of the different terms. Second order steps depend on the collision rate coefficient of their specific reactants as discussed in Section 3.2.2. They are observed to have a lower rate s^{-1} than the fastest first order reactions Fig 9 (b)-(d). This is expected as the first-order or unimolecular reactions are not limited by the concentration of a collision partner. Third order or higher reaction steps involve three or more reactants are observed to have the lowest rates s^{-1}, due to their use approximating a chain of multiple collisions. In this mechanism, there are relatively few third order reactions and most of them have a rate less than $1 s^{-1}$, so do not appear on this plot. Pressure dependent reaction steps such as three-body and falloff reactions have similar rates s^{-1} as second order steps. Finally, the summands for the temperature derivative terms also have relatively low rates s^{-1}. While a large term is not necessarily a problem, each excessively large element of the Jacobian Eq. (15) may be the result of a reaction step with a characteristic timescale that is faster than is practical or even physically possible, so their appearance could indicate an issue.

Figures 9 (a)-(d) show that the terms that make up the Jacobian for the n-heptane mechanism [41] are ordered as expected. To demonstrate some of the issues this analysis can uncover, we now analyze a large bio diesel mechanism [5] with 3,299 species and 10,805 reactions. We again carry out an ignition delay calculation with an initial temperature and pressure of 800 K and 20 bar, respectively. The temperature and pressure history during the ignition delay calculation are shown in Fig.10 (a). Low temperature ignition was found to occur at 0.534 ms and high temperature ignition at 0.954 ms. Similar to Fig. 9, the plots in Figs 10 (b)-(d) show the distribution of Jacobian summands at the time of low temperature ignition, hot ignition and after hot ignition.

Comparing the plots in Fig. 9 and Fig. 10 we can see that the biodiesel mechanism has a number of Jacobian summands above $10^{14} s^{-1}$ whereas the n-heptane did not. Of most concern are the third order or greater reactions since these are expected to occur at low rates, but there is a reaction with a rate s^{-1} greater than $10^{20} s^{-1}$ and a few reactions in the post ignition stage (Fig. 10 (d)) greater than $10^{7} s^{-1}$. Additionally, after ignition there are a number of second order reactions that have rates s^{-1} of $10^{12} s^{-1}$, above that of most of the first order reactions. By examining the Jacobian terms in more detail, we can identify the offending reactions and correct the rates and species thermochemistry as necessary. Often anomalously large frequen-

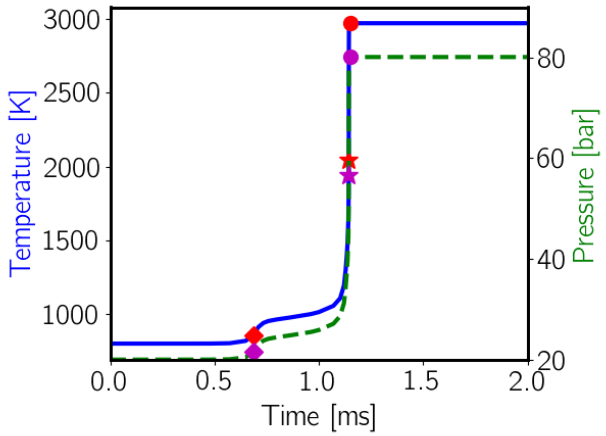

(a)

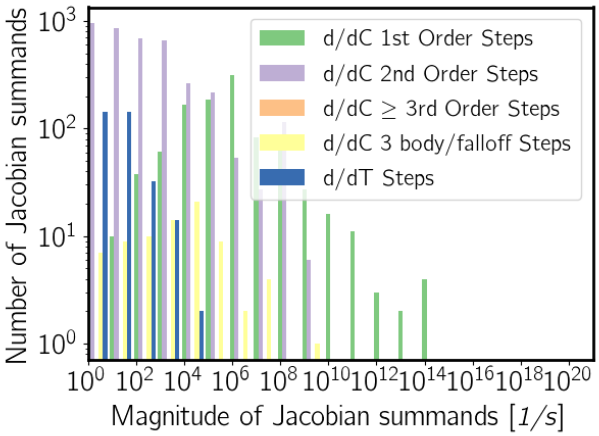

(b)

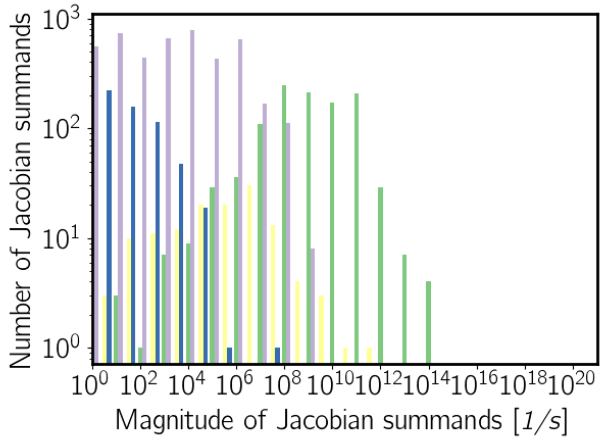

(c)

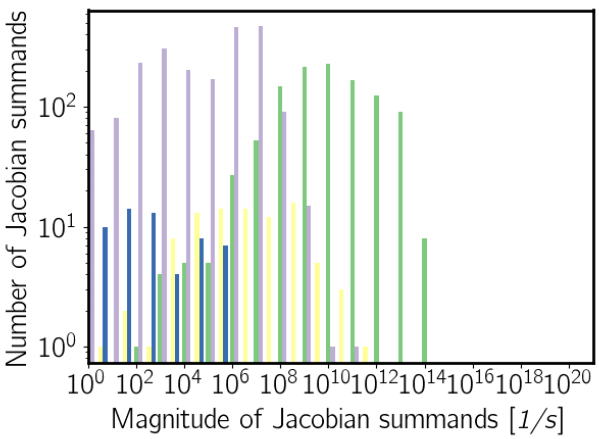

(d)

Figure 9: Jacobian analysis of detailed n-heptane mechanism [41].Temperature and pressure history during an ignition delay calculation with a stoichiometric mixture of n-heptane and air initiated at 800K and 20 bar in (a). The number of Jacobian summands are binned by magnitude at low temperature ignition (t=0.686 ms) in (b), during hot ignition (t=1.143 ms) in (c) and after ignition (t=1.152 ms) in (d).

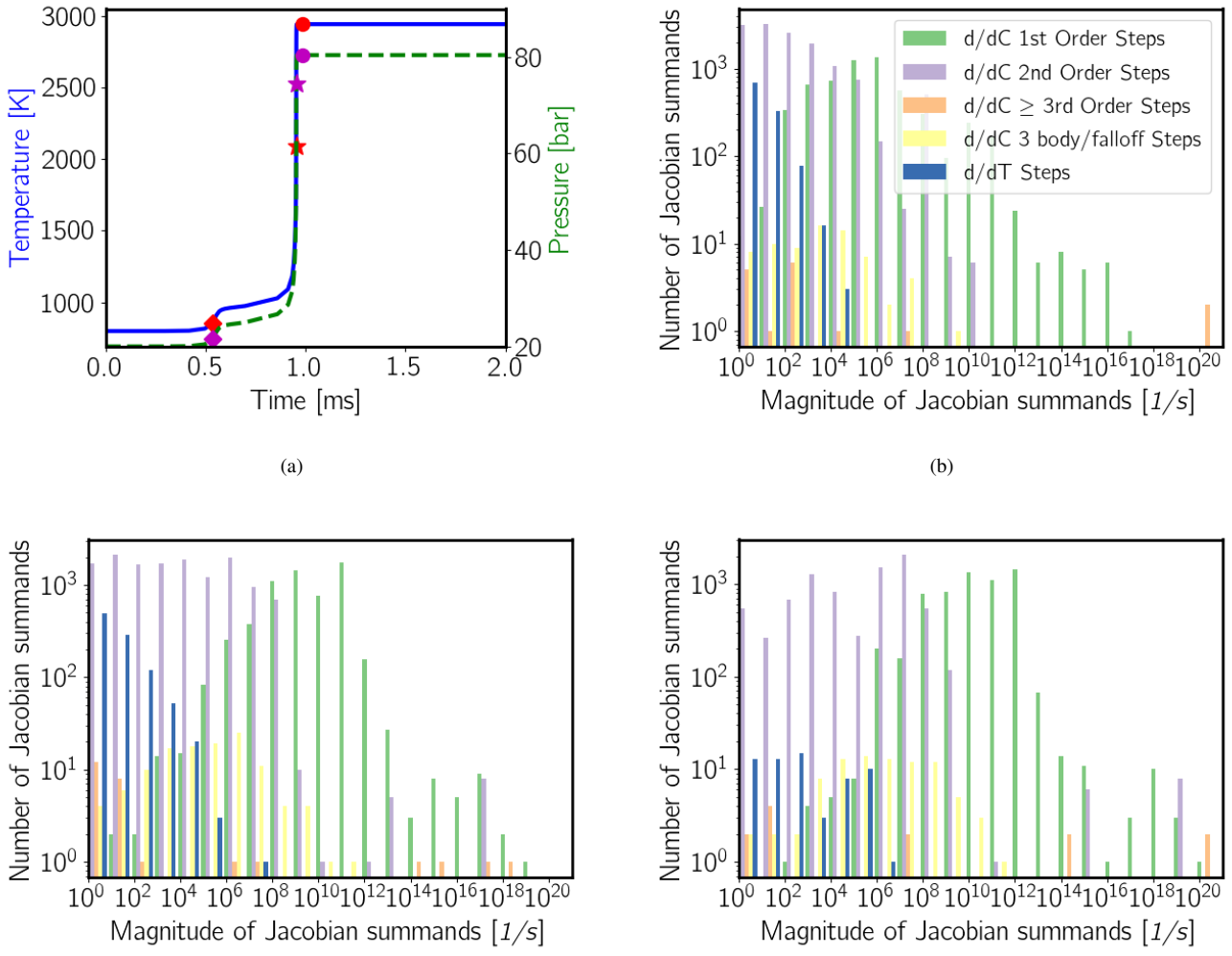

(a) (b)

(c) (d)

Figure 10: Jacobian analysis of detailed biodiesel mechanism [5].Temperature and pressure history during an ignition delay calculation with a stoichiometric mixture of methyl decanoate and air initiated at 800K and 20 bar in (a). The number of Jacobian summands are binned by rate s^{-1} at low temperature ignition (t=0.534 ms) in (b), during hot ignition (t=0.954 ms) in (c) and after ignition (t=0.986 ms) in (d).

cies for third-order (and higher) reactions are caused by reverse reaction rates being calculated from the equilibrium constant using the thermodynamic definitions specified with the mechanism. As a consequence, it is recommended that the thermodynamics of the reactants and products be inspected by the techniques in Section 2 with particular focus on the enthalpy and entropy values at 298.15 K.

4. Conclusions

The chemical mechanisms that describe combustion have become increasingly large as our physical understanding of the elementary reaction steps have improved and as computer resources have grown. As the size of these mechanisms grow it becomes increasingly difficult to proof them by hand and automated checks are needed to ensure they do not contain errors. This paper attempts to address this need by describing a number of basic checks for the thermodynamic files and mechanism files. It is shown that discontinuities in thermodynamic data can result in longer time to solution as solvers take smaller time steps to traverse them. A method to remove these discontinuities is demonstrated and shown to give near identical results as the original thermodynamic data, but with a lower computation cost. A number of checks for chemical mechanisms are also presented,

1. *Basic Checks* can be performed in which the number of reactants in each reaction are tabulated, and species are flagged that may have odd behavior in the context of the mechanism as it is formulated.
2. *Unimolecular Reaction Rate coefficients* are compared versus a threshold determined using transition state theory.
3. *Binary Reaction Rate coefficients* that exceed the binary collision limit are flagged.
4. *Jacobian Analysis* is used to check the time scales of higher order steps not covered by the other checks.

These checks have been implemented in a web-based application `https://combustiontools.llnl.gov` that allows users to quickly and easily check their mechanisms. We hope that this work will accelerate the process of detailed mechanism development, reduce time to solution when these mechanisms are integrated and weed out typos and non-physical errors that are otherwise difficult to identify due to the sheer size of detailed mechanisms.

Acknowledgments

The authors would like to thank John Consolati, Anthony Epshteyn, and Alejandro Dominguez for their help with designing and implementing the web application. This work was fully supported by the U.S. Department of Energy (DOE), Office of Energy Efficiency and Renewable Energy (EERE), Vehicle Technologies Office (VTO) under contract no. DE-AC52-07NA27344.

[1] R. Hilbert, F. Tap, H. El-Rabii, D. Thévenin, Impact of detailed chemistry and transport models on turbulent combustion simulations, Progress in Energy and Combustion Science 30 (1) (2004) 61–117.

[2] H. Pitsch, Large-eddy simulation of turbulent combustion, Annu. Rev. Fluid Mech. 38 (2006) 453–482.

[3] M. J. McNenly, R. A. Whitesides, D. L. Flowers, Faster solvers for large kinetic mechanisms using adaptive preconditioners, Proceedings of the Combustion Institute 35 (1) (2015) 581 – 587. doi:https://doi.org/10.1016/j.proci.2014.05.113.
URL http://www.sciencedirect.com/science/article/pii/S1540748914001163

[4] T. Lu, C. K. Law, Toward accommodating realistic fuel chemistry in large-scale computations, Progress in Energy and Combustion Science 35 (2) (2009) 192 – 215. doi:https://doi.org/10.1016/j.pecs.2008.10.002.
URL http://www.sciencedirect.com/science/article/pii/S036012850800066X

[5] O. Herbinet, W. J. Pitz, C. K. Westbrook, Detailed chemical kinetic mechanism for the oxidation of biodiesel fuels blend surrogate, Combustion and Flame 157 (5) (2010) 893–908.

[6] T. Turányi, A. S. Tomlin, Analysis of kinetic reaction mechanisms, Springer, 2014.

[7] D. Chen, K. Wang, H. Wang, Violation of collision limit in recently published reaction models, Combustion and Flame 186 (Supplement C) (2017) 208 – 210. doi:https://doi.org/10.1016/j.combustflame.2017.08.005.
URL http://www.sciencedirect.com/science/article/pii/S0010218017303024

[8] K. K. Yalamanchi, E.-A. Tingas, H. G. Im, S. M. Sarathy, Screening gas-phase chemical kinetic models: Collision limit compliance and ultrafast timescales, International Journal of Chemical Kinetics.

[9] S. K. Sirumalla, M. A. Mayer, K. E. Niemeyer, R. H. West, Assessing impacts of discrepancies in model parameters on autoignition model performance: A case study using butanol, Combustion and Flame 190 (2018) 284–292.

[10] M. Frenklach, Transforming data into knowledge–process informatics for combustion chemistry, Proceedings of the Combustion Institute 31 (1) (2007) 125 – 140. doi:https://doi.org/10.1016/j.proci.2006.08.121.
URL http://www.sciencedirect.com/science/article/pii/S1540748906003841

[11] G. L. Goteng, N. Nettyam, S. M. Sarathy, CloudFlame: Cyberinfrastructure for combustion research, in: Information Science and Cloud Computing Companion (ISCC-C), 2013 International Conference on, IEEE, 2013, pp. 294–299.

[12] N. Atef, G. Kukkadapu, S. Y. Mohamed, M. A. Rashidi, C. Banyon, M. Mehl, K. A. Heufer, E. F. Nasir, A. Alfazazi, A. K. Das, C. K. Westbrook, W. J. Pitz, T. Lu, A. Farooq, C.-J. Sung, H. J. Curran, S. M. Sarathy, A comprehensive iso-octane combustion model with improved thermochemistry and chemical kinetics, Combustion and Flame 178 (Supplement C) (2017) 111 – 134. doi:https://doi.org/10.1016/j.combustflame.2016.12.029.
URL http://www.sciencedirect.com/science/article/pii/S0010218016304059

[13] F. vom Lehn, L. Cai, H. Pitsch, Sensitivity analysis, uncertainty quantification, and optimization for thermochemical properties in chemical kinetic combustion models, Proceedings of the Combustion Institute 37 (1) (2019) 771 – 779. doi:https://doi.org/10.1016/j.proci.2018.06.188.
URL http://www.sciencedirect.com/science/article/pii/S1540748918303742

[14] N. Morgan, A. Smallbone, A. Bhave, M. Kraft, R. Cracknell, G. Kalghatgi, Mapping surrogate gasoline compositions into RON/MON space, Combustion and Flame 157 (6) (2010) 1122–1131.

[15] J. C. Andrae, T. Brinck, G. T. Kalghatgi, HCCI experiments with toluene reference fuels modeled by a semidetailed chemical kinetic model, Combustion and Flame 155 (4) (2008) 696–712.

[16] P. Boettcher, R. Mével, V. Thomas, J. Shepherd, The effect of heating rates on low temperature hexane air combustion, Fuel 96 (2012) 392–403.

[17] A. Cuoci, A. Frassoldati, T. Faravelli, E. Ranzi, OpenSMOKE++: An object-oriented framework for the numerical modeling of reactive sys-

tems with detailed kinetic mechanisms, Computer Physics Communications 192 (2015) 237–264.
[18] B. J. McBride, S. Gordon, Computer program for calculation of complex chemical equilibrium compositions and applications, Tech. rep., NASA (1996).
[19] E. Goos, G. Lendvay, Calculation of molecular thermochemical data and their availability in databases, in: Cleaner Combustion, Springer, 2013, pp. 515–547.
[20] I. Glassman, R. A. Yetter, N. G. Glumac, Combustion, Academic press, 2014.
[21] J. Kodavasal, M. J. McNenly, A. Babajimopoulos, S. M. Aceves, D. N. Assanis, M. A. Havstad, D. L. Flowers, An accelerated multi-zone model for engine cycle simulation of homogeneous charge compression ignition combustion, International Journal of Engine Research 14 (5) (2013) 416–433. arXiv:https://doi.org/10.1177/1468087413482480, doi:10.1177/1468087413482480.
URL https://doi.org/10.1177/1468087413482480
[22] S. Goldsborough, M. Johnson, C. Banyon, W. Pitz, M. McNenly, Experimental and modeling study of fuel interactions with an alkyl nitrate cetane enhancer, 2-ethyl-hexyl nitrate, Proceedings of the Combustion Institute 35 (1) (2015) 571 – 579. doi:https://doi.org/10.1016/j.proci.2014.06.048.
URL http://www.sciencedirect.com/science/article/pii/S1540748914002065
[23] P. J. Linstrom, W. G. Mallard, The NIST chemistry webbook: a chemical data resource on the internet, Journal of Chemical & Engineering Data 46 (5) (2001) 1059–1063. arXiv:https://doi.org/10.1021/je000236i, doi:10.1021/je000236i.
URL https://doi.org/10.1021/je000236i
[24] S. Snitsiriwat, J. W. Bozzelli, Thermochemical properties for isooctane and carbon radicals: computational study, The Journal of Physical Chemistry A 117 (2) (2013) 421–429.
[25] J. M. Hudzik, J. W. Bozzelli, J. M. Simmie, Thermochemistry of C7H16 to C10H22 alkane isomers: primary, secondary, and tertiary C–H bond dissociation energies and effects of branching, The Journal of Physical Chemistry A 118 (40) (2014) 9364–9379.
[26] B. Ruscic, D. H. Bross, Active Thermochemical Tables (ATcT), https://atct.anl.gov (2019).
[27] S. W. Benson, J. H. Buss, Additivity rules for the estimation of molecular properties. thermodynamic properties, The Journal of Chemical Physics 29 (3) (1958) 546–572.
[28] S. W. Benson, F. Cruickshank, D. Golden, G. R. Haugen, H. O'Neal, A. Rodgers, R. Shaw, R. Walsh, Additivity rules for the estimation of thermochemical properties, Chemical Reviews 69 (3) (1969) 279–324.
[29] O. Herbinet, W. J. Pitz, C. K. Westbrook, Detailed chemical kinetic oxidation mechanism for a biodiesel surrogate, Combustion and Flame 154 (3) (2008) 507–528.
[30] A. Fernández-Ramos, J. A. Miller, S. J. Klippenstein, D. G. Truhlar, Modeling the kinetics of bimolecular reactions, Chemical Reviews 106 (11) (2006) 4518–4584.
[31] W. G. Vincenti, C. H. Kruger, Introduction to physical gas dynamics, Introduction to physical gas dynamics, New York, Wiley.
[32] G. Bird, Molecular gas dynamics and the direct simulation Monte Carlo of gas flows, Clarendon, Oxford 508 (1994) 128.
[33] R. B. Bird, Transport phenomena, Applied Mechanics Reviews 55 (1) (2002) R1–R4.
[34] L. Monchick, E. Mason, Transport properties of polar gases, The Journal of Chemical Physics 35 (5) (1961) 1676–1697.
[35] R. A. Svehla, Estimated viscosities and thermal conductivities of gases at high temperatures, Tech. rep., National Aeronautics and Space Administration. Lewis Research Center, Cleveland (1962).
[36] H. Wang, M. Frenklach, Transport properties of polycyclic aromatic hydrocarbons for flame modeling, Combustion and Flame 96 (1) (1994) 163 – 170. doi:https://doi.org/10.1016/0010-2180(94)90167-8.
URL http://www.sciencedirect.com/science/article/pii/0010218094901678
[37] A. Babajimopoulos, D. N. Assanis, D. L. Flowers, S. M. Aceves, R. P. Hessel, A fully coupled computational fluid dynamics and multi-zone model with detailed chemical kinetics for the simulation of premixed charge compression ignition engines, International Journal of Engine Research 6 (5) (2005) 497–512. arXiv:https://doi.org/10.1243/146808705X30503, doi:10.1243/146808705X30503.
URL https://doi.org/10.1243/146808705X30503
[38] M. Raju, M. Wang, M. Dai, W. Piggott, D. Flowers, Acceleration of detailed chemical kinetics using multi-zone modeling for CFD in internal combustion engine simulations, Tech. rep., SAE Technical Paper (2012).
[39] K. K. Kuo, Principles of combustion, John Wiley & Sons, Inc., 2005.
[40] L. N. Trefethen, D. Bau III, Numerical linear algebra, Vol. 50, Siam, 1997.
[41] M. Mehl, W. J. Pitz, C. K. Westbrook, H. J. Curran, Kinetic modeling of gasoline surrogate components and mixtures under engine conditions, Proceedings of the Combustion Institute 33 (1) (2011) 193–200.